*The Journal of Engineering*

WILEY

IET The Institution of Engineering and Technology

ORIGINAL RESEARCH OPEN ACCESS

# Efficiency Improvement of a 10 W GaN HEMT Power Amplifier Based on Hidden Markov Model Optimized by Particle Swarm Optimization Algorithm for Wireless Application

Mohammad Soruri[1] | Patrizia Livreri[2]

[1]Faculty of Ferdows Technical, University of Birjand, Birjand, Iran | [2]Department of Engineering, University of Palermo, Palermo, Italy

**Correspondence:** Mohammad Soruri (mohamad.soruri@birjand.ac.ir)

**Received:** 19 September 2024 | **Revised:** 10 April 2025 | **Accepted:** 21 April 2025

**Funding:** The authors received no specific funding for this work.

## ABSTRACT

Power amplifier design is an important topic in communication systems. Improving the efficiency of a power amplifier has long been a key interest to RF designers. In this paper, a 10 W GaN HEMT power amplifier is designed based on Hidden Markov Model optimized by Particle Swarm Optimization. The widths and lengths of the microstrip lines at the input and output of the matching networks in the proposed power amplifier are modelled using the Hidden Markov Model. For training the parameters of the Hidden Markov Model, the Particle Swarm Optimization algorithm is used. The power amplifier utilizes a 10 W GaN HEMT transistor (model CG2H40010F from Cree Corporation) and operates over a bandwidth of 2.5–3 GHz. At 2.98 GHz, the power amplifier achieves an output power of 39.3 dBm, a power-added efficiency of 63.2%, and a gain of 15.3 dB. Across the entire bandwidth, it maintains output power above 38.18 dBm and gain above 14.2 dB, with power-added efficiency exceeding 50% between 2.8 and 3 GHz. These results highlight the effectiveness of the HMM-PSO approach in enhancing the performance of the proposed GaN HEMT power amplifier.

## 1 | Introduction

Power amplifiers (PAs) are found in the final stage of the RF transmitter chain [1]. As the input signal is large, the type of structure of a PA can have a significant effect on the overall efficiency of the transmitter [1, 2]. Therefore, numerous efforts are made to ensure that the structure of a power amplifier has the best match, thereby achieving its optimal efficiency.

Optimizing a PA is an important issue for improving its efficiency. There are several conventional techniques such as switching power amplifiers and Doherty power amplifiers [3], the envelope tracking (ET) [4] and the outphasing technique [5] for obtaining acceptable parameters from a PA. In recent years, innovative and evolutionary algorithms for optimizing the discrete PA (DPA) and monolithic microwave integrated circuits (MMIC) have also been developed. As the power amplifier design is faced with several conflicting parameters such as efficiency, linearity and output power, multi-objective optimization can help achieve acceptable results from a PA [6].

So far, several optimization algorithms have been proposed for PA optimization. The inclined planes system optimization (IPO) algorithm was presented for the design of a discrete power amplifier in [7]. Particle swarm optimization (PSO) was used for the optimization of several PAs in [8–11]. Also in [12], a combination

of artificial bee colony (ABC) and PSO algorithms were applied by Bipin and Rao for the linearization of a PA. A nonlinear programming technique was applied for the optimization of a PA in [13]. Bayesian optimization and automated deep neural learning were studied for improving the efficiency and gain in [14] and [15] over the frequency range of 1.5–2.5 GHz and 1.8–2.2 GHz, respectively. Also, simulated annealing with particle swarm optimization for high-efficiency power amplifier design was worked in [11].

In this paper, the hidden Markov model (HMM) is used for modelling the PA. For training the parameters of HMM, the PSO algorithm is applied. The PSO algorithm is a robust algorithm that was introduced by Kennedy and Eberhart in 1995 [16]. In the proposed approach, the widths and lengths of microstrips are modelled by HMM optimized by the PSO algorithm so that the best match for amplifiers can be obtained. The rest of the paper is organized as follows: Section 2 introduces the proposed algorithm, which includes Section 2.1 for describing HMM modelling and Section 2.2 for describing PSO optimization. The results are presented in Section 3, and the conclusion is drawn in Section 4.

## 2 | Proposed Algorithm

In this section, PA modelling with HMM and optimizing its parameters with the PSO algorithm are described. Initially, we should obtain a model for PA.

### 2.1 | PA Modelling with HMM

The parameters of the proposed PA for optimization are the widths and lengths of the microstrip lines in the input and output of the matching networks. Figure 1 shows the schematic of the proposed structure of PA, which is modelled and optimized using HMM and PSO.

As seen in Figure 1, there are 9 microstrip lines in the input matching network and 9 microstrip lines in the output matching network. $R_S$ and $C_S$, which are parallel resistor and capacitor located on the gate side, are chosen in such a way that stability is guaranteed at all frequencies. Also, to provide more stability of PA in Figure 1, the two first microstrip lines from the gate side, whose widths and lengths are specified by $W_{g_1}, L_{g_1}, W_{g_2}, L_{g_2}$ and the two first microstrip lines from the drain side, whose widths and lengths are specified by $W_{d_1}, L_{d_1}, W_{d_2}, L_{d_2}$, are chosen and fixed. Other widths and lengths of the microstrip lines in the proposed PA, should be optimized by the optimization algorithm. So, the vectors of $S_i, S_o$ and $S$ can be realized by the following equations.

$$S_{i(1-7)} = \left[W_{i_1}, L_{i_1}, W_{i_2}, L_{i_2}, W_{i_3}, L_{i_3}, W_{i_4}, L_{i_4}, W_{i_5}, L_{i_5}, W_{i_6}, L_{i_6}, W_{i_7}, L_{i_7}\right] \quad (1)$$

$$S_{o(1-7)} = \left[W_{o_1}, L_{o_1}, W_{o_2}, L_{o_2}, W_{o_3}, L_{o_3}, W_{o_4}, L_{o_4}, W_{o_5}, L_{o_5}, W_{o_6}, L_{o_6}, W_{o_7}, L_{o_7}\right] \quad (2)$$

$$S = \left[S_{i(1-7)}, S_{o(1-7)}\right] \quad (3)$$

Where in Equations (1) and (2), $S_i$ and $S_o$ are the widths and lengths of the 7 microstrip lines in the input and the output of matching networks, respectively. Equation (3) shows that the vectors of $S_i$ and $S_o$ are merged into the vector of $S$. Therefore, $S$ is a vector of 28 parameters that the proposed algorithm should optimize.

Each HMM can be shown with a triple parameter of $\lambda = (A,B,\pi)$ that specifies the overall specification of the model [17, 18]. $A$ is the transition, $B$ is the emission and $\pi$ is the initial matrix. Figure 2 shows a simple structure of HMM.

In Figure 2, HMM consists of two hidden states ($H_1$,$H_2$) and three observable states ($O_1$,$O_2$,$O_3$). As seen in Figure 2, each hidden state can emit three observable states. In HMM, the probability of transitioning from one hidden state to another is specified by the transition probability, and the emission probability specifies the probability of emitting an observable state from a hidden state. In Figure 2, the transition probabilities and emission probabilities are represented by dotted lines and solid lines, respectively.

Assuming that HMM consists of $n$ hidden states and $m$ observable states, transition, emission and initial probabilities can be stated by the following equations [17].

$$a_{ij} = P\left(\pi_j(t+1) \,|\pi_i(t)\right) 1 < i, j < n \quad (4)$$

$$b_{jk} = P\left(\upsilon_k(t) \,|\pi_j(t)\right) 1 < j < n, 1 < k < m \quad (5)$$

$$\pi_i = P\left(\pi(1) = \pi_i(1)\right), 1 < i < n \quad (6)$$

Where in Equation (4), $a_{ij}$ is the transition probability from the current hidden state, $\pi_i(t)$, to the next hidden state, $\pi_j(t+1)$. In Equation (5), $b_{jk}$ is the probability of generating the observable state, $\upsilon_k(t)$ from the hidden state, $\pi_j(t)$ and in Equation (6), the probability of starting the model with a hidden state of $\pi(1)$, is equal to $\pi_i$.

### 2.2 | Optimization of HMM With PSO

For optimizing the HMM with PSO, transition probabilities are considered as the particles in the PSO algorithm. For a more detailed description of the particle structure, the model used for HMM is illustrated in Figure 3.

As seen in Figure 3, the HMM has 28 hidden states and each hidden state can emit 10 observable states. The reason for using 28 hidden modes is that the number of microstrip lines that should be optimized in the structure of PA is 14 and each microstrip has two parameters of width and length, hence, the total number of widths and lengths of microstrip lines for optimizing are 28 [19]. Also, as shown in Figure 3, each hidden state can emit 10 observable states and the values of these 10 observable states are obtained from the load-pull simulation and an initial tuning for achieving the maximum efficiency. Based on Figure 3, the transition matrix and emission matrix can be obtained by Equations (7) and (8), respectively [19].

$$\begin{bmatrix}
0&1&0&0&0&0&0&0&0&0&0&0&0&0&0&0&0&0&0&0&0&0&0&0&0&0&0&0\\
0&0&1&0&0&0&0&0&0&0&0&0&0&0&0&0&0&0&0&0&0&0&0&0&0&0&0&0\\
0&0&0&1&0&0&0&0&0&0&0&0&0&0&0&0&0&0&0&0&0&0&0&0&0&0&0&0\\
0&0&0&0&1&0&0&0&0&0&0&0&0&0&0&0&0&0&0&0&0&0&0&0&0&0&0&0\\
0&0&0&0&0&1&0&0&0&0&0&0&0&0&0&0&0&0&0&0&0&0&0&0&0&0&0&0\\
0&0&0&0&0&0&1&0&0&0&0&0&0&0&0&0&0&0&0&0&0&0&0&0&0&0&0&0\\
0&0&0&0&0&0&0&1&0&0&0&0&0&0&0&0&0&0&0&0&0&0&0&0&0&0&0&0\\
0&0&0&0&0&0&0&0&1&0&0&0&0&0&0&0&0&0&0&0&0&0&0&0&0&0&0&0\\
0&0&0&0&0&0&0&0&0&1&0&0&0&0&0&0&0&0&0&0&0&0&0&0&0&0&0&0\\
0&0&0&0&0&0&0&0&0&0&1&0&0&0&0&0&0&0&0&0&0&0&0&0&0&0&0&0\\
0&0&0&0&0&0&0&0&0&0&0&1&0&0&0&0&0&0&0&0&0&0&0&0&0&0&0&0\\
0&0&0&0&0&0&0&0&0&0&0&0&1&0&0&0&0&0&0&0&0&0&0&0&0&0&0&0\\
0&0&0&0&0&0&0&0&0&0&0&0&0&1&0&0&0&0&0&0&0&0&0&0&0&0&0&0\\
0&0&0&0&0&0&0&0&0&0&0&0&0&0&1&0&0&0&0&0&0&0&0&0&0&0&0&0\\
0&0&0&0&0&0&0&0&0&0&0&0&0&0&0&1&0&0&0&0&0&0&0&0&0&0&0&0\\
0&0&0&0&0&0&0&0&0&0&0&0&0&0&0&0&1&0&0&0&0&0&0&0&0&0&0&0\\
0&0&0&0&0&0&0&0&0&0&0&0&0&0&0&0&0&1&0&0&0&0&0&0&0&0&0&0\\
0&0&0&0&0&0&0&0&0&0&0&0&0&0&0&0&0&0&1&0&0&0&0&0&0&0&0&0\\
0&0&0&0&0&0&0&0&0&0&0&0&0&0&0&0&0&0&0&1&0&0&0&0&0&0&0&0\\
0&0&0&0&0&0&0&0&0&0&0&0&0&0&0&0&0&0&0&0&1&0&0&0&0&0&0&0\\
0&0&0&0&0&0&0&0&0&0&0&0&0&0&0&0&0&0&0&0&0&1&0&0&0&0&0&0\\
0&0&0&0&0&0&0&0&0&0&0&0&0&0&0&0&0&0&0&0&0&0&1&0&0&0&0&0\\
0&0&0&0&0&0&0&0&0&0&0&0&0&0&0&0&0&0&0&0&0&0&0&1&0&0&0&0\\
0&0&0&0&0&0&0&0&0&0&0&0&0&0&0&0&0&0&0&0&0&0&0&0&1&0&0&0\\
0&0&0&0&0&0&0&0&0&0&0&0&0&0&0&0&0&0&0&0&0&0&0&0&0&1&0&0\\
0&0&0&0&0&0&0&0&0&0&0&0&0&0&0&0&0&0&0&0&0&0&0&0&0&0&1&0\\
0&0&0&0&0&0&0&0&0&0&0&0&0&0&0&0&0&0&0&0&0&0&0&0&0&0&0&1\\
1&0&0&0&0&0&0&0&0&0&0&0&0&0&0&0&0&0&0&0&0&0&0&0&0&0&0&0
\end{bmatrix}_{28\times 28} \tag{7}$$

$$B=\begin{bmatrix} b_{1,1} & . & . & b_{1,10}\\ . & & & \\ . & & & \\ b_{28,1} & . & . & b_{28,10}\end{bmatrix}_{28\times 10} \tag{8}$$

As seen in Equation (7), the values of transition matrix A are fixed and supposing that the algorithm starts at the hidden state of $\pi(1)$, the initial matrix can be stated as follows:

$$\pi=[1\,0\,0\,0\,0\,0\,0\,0\,0\,0\,0\,0\,0\,0\,0\,0\,0\,0\,0\,0\,0\,0\,0\,0\,0\,0\,0\,0] \tag{9}$$

In the HMM training with the PSO algorithm, particles are emission matrices that are produced at the beginning of the PSO algorithm [18]. In this case, the values of the transition matrix and initial matrix, as shown in Equation (7) and (8), respectively, are fixed. In other words, for training the HMM, the PSO algorithm should optimize only the emission matrix. Equation (10) shows the formation of a particle structure from the emission matrix B:

$$B=\begin{bmatrix} b_{1,1} & . & . & b_{1,10}\\ . & & & \\ . & & & \\ b_{28,1} & . & . & b_{28,10}\end{bmatrix}_{28\times 10}$$

$$\longrightarrow P=(\mathrm{b}_{1,1},\mathrm{b}_{1,2},\mathrm{b}_{1,3},\mathrm{b}_{1,4},\mathrm{b}_{1,5},\ldots,\mathrm{b}_{28,8},\mathrm{b}_{28,9},\mathrm{b}_{28,10}) \tag{10}$$

As seen in Equation (10), each particle has 280 dimensions in the search space. To validate the emission matrix of B, the condition that the sum of the probabilities of each row must be checked in each iteration of the PSO algorithm. Equation (11) shows this condition:

$$\sum_{k=1}^{10} b_{fk}=1, 1<f<28 \tag{11}$$

After determining the structure of each particle, the fitness function of the PSO algorithm is defined. To obtain the fitness function, the concept of maximum likelihood is employed. Equation (12) determines the fitness function:

$$F=P(S|\lambda) \tag{12}$$

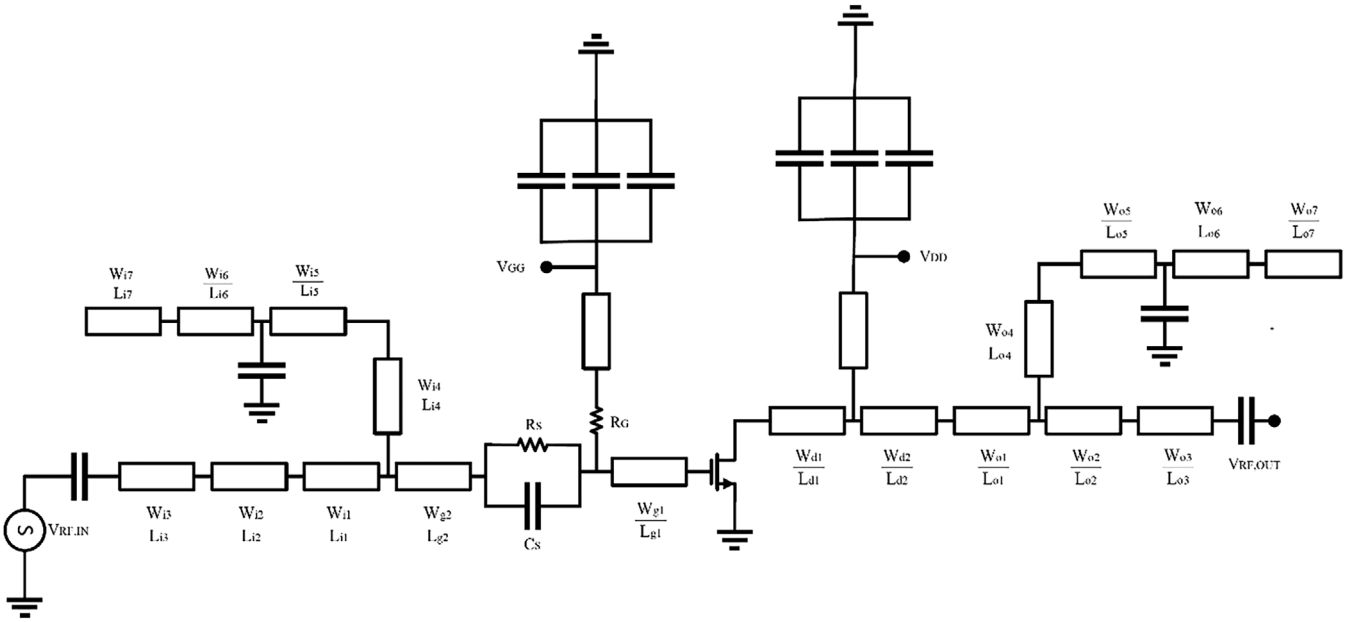


**FIGURE 1** | Schematics of the proposed PA for modelling by HMM trained with PSO.

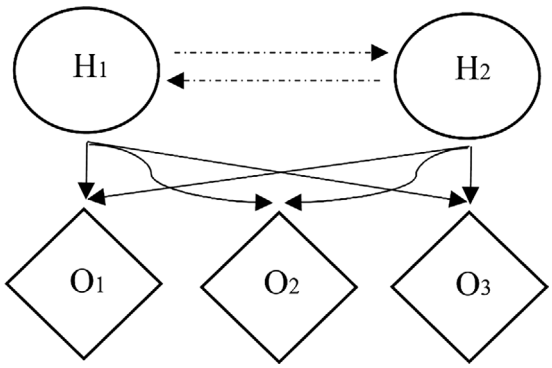


**FIGURE 2** | A simple structure of HMM.

Where in Equation (12), $\lambda = (A,B,\pi)$ describes the proposed HMM and $F$ is the maximum posterior probability of generating the sequence $S$ by $\lambda$ [17]. It should be noted that to obtain $\lambda$, the emission matrix of B is extracted from the particle $P$, while the matrices of A and $\pi$ are fixed, as mentioned in Equation (7) and (9). The PSO algorithm is run to train the HMM and terminated when the obtained error is below a threshold value or the maximum number of iterations is reached.

## 3 | Results and Discussion

In the proposed PA structure shown in Figure 1, a 10 W GaN HEMT with part number CG2H40010F from Cree Corporation is utilized. The supply voltage of the drain is 28 V and the drain current is 100 mA. For HMM modelling and training with the PSO algorithm, MATLAB is used which is linked with ADS software for implementation of the harmonic balance simulations of the PA [20, 21]. Rogers 4003 with a thickness of 32 mils and $\varepsilon_r = 3.55$ is used as the substrate of the PA. Because the primary goal of designing PA is to achieve maximum efficiency, the deep AB class is chosen for biasing PA. Figure 4 shows the Mu factor of PA.

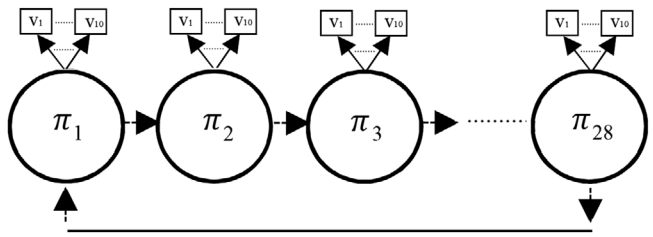


**FIGURE 3** | The model of HMM used for training with PSO.

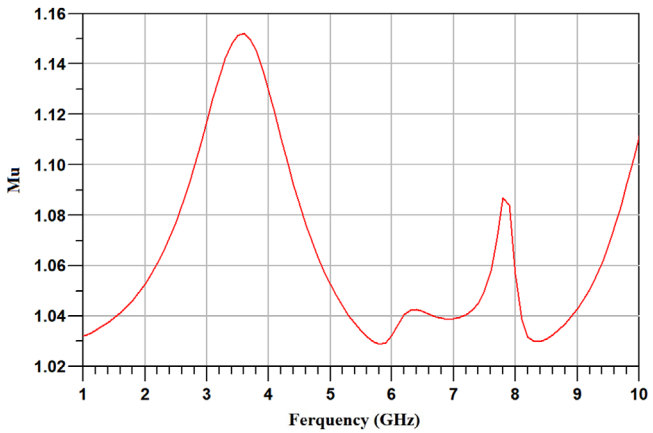


**FIGURE 4** | The Mu factor of PA.

As seen in Figure 4, the values of the Mu factor are greater in the frequency range of 1 to 10 GHz and so the stability is guaranteed over the bandwidth of PA. Tables 1 and 2 show the optimized values of the microstrip lines obtained from the HMM model trained by the PSO algorithm.

Figures 5 and 6 Show $S_{11}$ and $S_{22}$ of the PA, respectively. As shown, $S_{11}$ and $S_{22}$ are lower than −10 dB in the range of 2.5 to 3 GHz,

**TABLE 1** | Optimized values of 7 microstrip lines in the input matching network obtained from the HMM model trained by the PSO algorithm (All values are in millimetres).

| $W_{i(1-7)}$ | 2.8 | 2.9 | 2 | 1.5 | 8.73 | 0.8 | 13 | 10 | 7.27 | 14.5 | 5.8 | 8.6 | 4.3 | 3.1 |
|---|---|---|---|---|---|---|---|---|---|---|---|---|---|---|
| $L_{i(1-7)}$ | 1.6 | 3.4 | 14 | 13.89 | 6.39 | 1.2 | 8 | 14.63 | 7.43 | 2 | 3.5 | 4.5 | 2.6 | 5.6 |

**TABLE 2** | Optimized values of 7 microstrip lines in the output matching obtained from the HMM model trained by the PSO algorithm (All values are in millimetres).

| $W_{o(1-7)}$ | 6.9 | 4.4 | 1.9 | 3.5 | 4.1 | 1.5 | 4.3 | 3.6 | 5.2 | 8.2 | 6.5 | 5.3 | 2.8 | 4 |
|---|---|---|---|---|---|---|---|---|---|---|---|---|---|---|
| $L_{o(1-7)}$ | 3.4 | 5.3 | 2.3 | 2.6 | 2.8 | 2.8 | 5.2 | 4.2 | 4.3 | 4.5 | 5.6 | 3.7 | 5.2 | 3.2 |

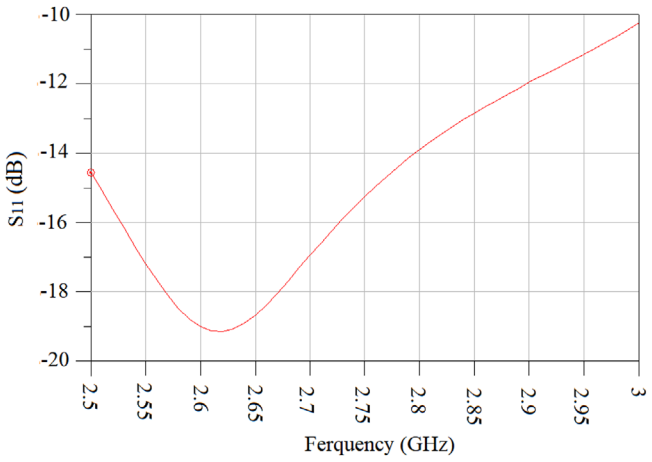


**FIGURE 5** | $S_{11}$ of the proposed PA versus frequency.

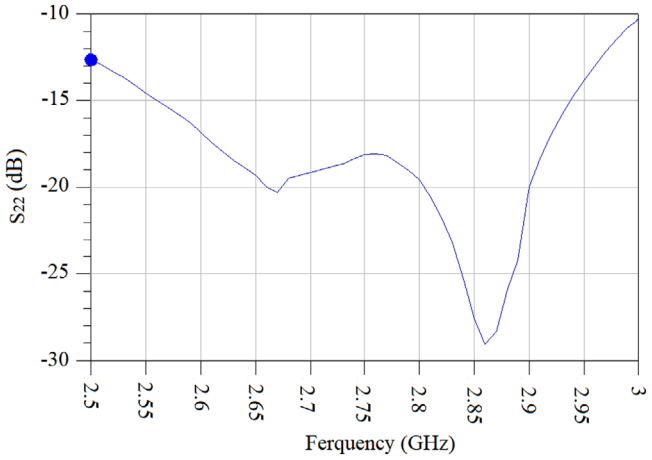


**FIGURE 6** | $S_{22}$ of the proposed PA versus frequency.

indicating that the results of the input and output matching networks are in good agreement.

In Figure 7, PAE, gain, and $P_{out}$ are shown together versus frequency at $P_{in}$ of 24 dBm. Carefully in the results shown in Figure 7, these points can be obtained:

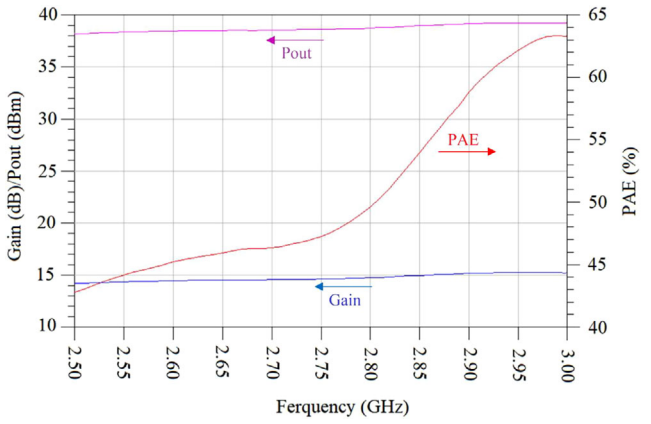


**FIGURE 7** | PAE, $P_{out}$, and Gain versus frequency at $P_{in}$ of 24 dBm.

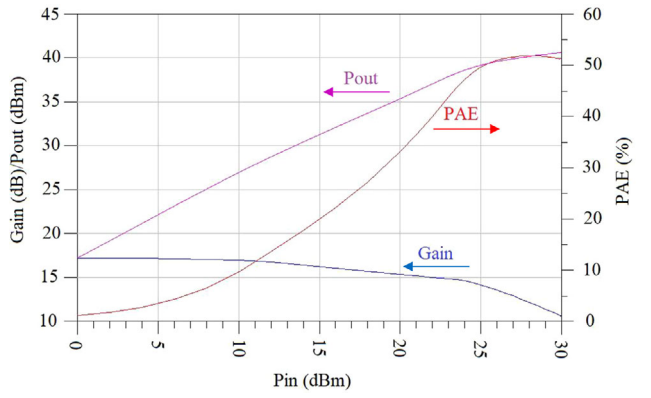


**FIGURE 8** | PAE, Pout, and Gain versus Pin at the frequency of 2.75 GHz.

A. The PAE of the proposed PA is above 43% in the whole bandwidth range. Also, PAE is above 50% in the frequency range of 2.8 to 3 GHz.

B. The Gain parameter is above 14.15 dB in the whole bandwidth range and is above 14.7 dB in the frequency range of 2.8 to 3 GHz. Additionally, the parameter of $P_{out}$ is above 38.1 and 39.2 dBm in the frequency range of 2.5 to 3 GHz and 2.8 to 3 GHz, respectively.

Figure 8 shows the PAE, Gain, and $P_{out}$ of the proposed PA versus input power at the frequency of 2.75 GHz. As shown in Figure 8,

**TABLE 3** | Performance comparison of the proposed PA versus some previously published S-band PAs.

| Ref. / Parameters | Transistor model | Substrate | BW (GHz) | Gain (dB) | PAE(%) | $V_{DD}/I_{DSQ}$ | $P_{out}$ (dBm) | Complexity |
|---|---|---|---|---|---|---|---|---|
| [15] | Ampleon CLF1G0060-10 | RO4350B | 1.8–2.2 | 10.1–11.6 | 64.3–79.7 (DE) | 50 V/40 mA | 14.1–16.6 (W) | No |
| [19] | Cree CGH40010 | RO4003 | 1.8–2.5 | 13.9–15.8 | 50.25–65.2 | 28 V/160 mA | 38.4–39.7 | No |
| [22] | Cree CGH40010 | N/A | 2–4 | 12.3–14.1 | 36.5–53.4 | 28 V/200 mA | 40 | No |
| [23] | Cree CGH40010F | RO4350B | 1.9–2.9 | 10–12.5 | 37–69 | 28 V/220 mA | 36–40 | No |
| [24] | Cree CGH40010 | Taconic TLX-8 | 2–3 | 11.5–12.5 | 58–72 | 28/60 mA | N/A | Yes |
| [25] | Cree CGH40010 | RO4350B | 1.85–2.7 | 10–11.8 | 68–77(DE) | 28 V/155 mA | 40.3–41 | Yes |
| [26] | Cree (10 W) N/A | N/A | 2.3–2.7 | 12 | 57–66 | N/A | >40 | No |
| [27] | Mitsubishi MGF0840G | RO4350B | 1.65–2.75 | <14 | 55–72 (DE) | 47 V/90 mA | 39.5–41.5 | Yes |
| [28] | Cree CGH40010F | RO6035 | 2.7–3.2 | 10 | 47 | 28 V/200 mA | <40 | No |
| [29] | Cree CGH40010F | RO4350B | 1–2.5 | 12.3–14.1 | 48-55 | 28/340 mA | N/A | Yes |
| This work | Cree CGH40010F | RO4003 | 2.5–3 | 14.15–15.25 | 43-63 | 28 V/100 mA | 38.1–39.25 | No |




**FIGURE 9** | P_Fund and P_Third of proposed PA versus Pin at the frequency of 2.75 GHz.

in the saturation region, where the $P_{in}$ is between 25 and 30 dBm, the PAE exceeds 50% and reaches a maximum of 52% at a $P_{in}$ of 28 dBm. Also in the saturation region, the average of $P_{out}$ is 40 dBm and the maximum value of gain is 14.2 dB at the $P_{in}$ of 25 dBm. Fundamental power (P_Fund) and Third harmonic power (P_Third) versus Pin at the frequency of 2.75 GHz, are shown in Figure 9. As shown in Figure 9, in the Pin of 24 dBm P_Fund and P_Third reach up to 38.5 and 9.3 dBm, respectively.

Table 3 provides a concise comparison of the performance between the proposed PA and several previously published S-band PAs. As illustrated in Table 3, the proposed PA generally outperforms most other works, demonstrating improvements in PA performance, gain, and output power.

## 4 | Conclusion

This paper presents the design of a PA using HMM optimized via the PSO algorithm for wireless application. The structure of PA was modelled by HMM that consisted of 28 hidden states and each hidden state can emit 10 observable states. The emission matrix was trained and optimized with the PSO algorithm. The cost function of the optimization algorithm was based on the maximum likelihood concept, which specified the maximum posterior probability of generating the sequence of widths and lengths of the proposed PA by the HMM. After modelling and optimizing the HMM with the final optimum values of microstrip lines and a nonlinear model of the PA, harmonic balance simulations were applied to the optimized structure of the PA. The simulation results show that the proposed PA could achieve a high PAE, Gain, and output power over the frequency range of the bandwidth.

### Author Contributions

**Mohammad Soruri:** conceptualization, data curation, methodology, software, validation, formal analysis, resources, writing – original draft, writing – review & editing. **Patrizia Livreri:** supervision, investigation, resources, review & editing.

## Conflicts of Interest

The authors declare no conflicts of interest.

## Data Availability Statement

Data sharing not applicable to this article as no datasets were generated or analysed during the current study.

## References


1. P. Colantonio, F. Giannini, and E. Limiti, *High Efficiency RF and Microwave Solid State Power Amplifiers* (John Wiley & Sons, 2009).

2. M. K. Kazimierczuk, *RF Power Amplifiers*. 2rd ed. (John Wiley & Sons, 2014).

3. B. Kim, *Doherty Power Amplifiers: From Fundamentals to Advanced Design Methods*. 1st ed. (Academic Press, 2018).

4. J. Staudinger, B. Gilsdorf, D. Newman, et al., "High Efficiency CDMA RF Power Amplifier Using Dynamic Envelope Tracking Technique," in 2000 IEEE MTT-S International Microwave Symposium Digest (IEEE 2000), 873–876.

5. S. C. Cripps, *RF Power Amplifiers for Wireless Communications*. 2rd ed. (Artech House, 2006).

6. M. Bhuvaneswari, *Application of Evolutionary Algorithms for Multi-Objective Optimization in VLSI and Embedded Systems* (Springer, 2014).

7. M. Soruri, S. Razavi, and M. Forouzanfar, "Design and Optimizing of a GaN HEMT Power Amplifier Based on the Inclined Planes System Optimization Algorithm for Wireless Applications," *Iranian Journal of Electrical and Electronic Engineering* 18, no. 3 (2022): 2369–2369.

8. S. Manjula and D. Selvathi, "Design and Optimization of Ultra Low Power Low Noise Amplifier Using Particle Swarm Optimization," *Indian Journal of Science and Technology* 8, no. 36 (2015): 1–8.

9. S. A. Hosseini, A. Hajipour, and H. Tavakoli, "Design and Optimization of a CMOS Power Amplifier Using Innovative Fractional-Order Particle Swarm Optimization," *Applied Soft Computin* 85 (2019): 105831.

10. G. Karimi and A. Lotfi, "An Analog/Digital Pre-Distorter Using Particle Swarm Optimization for RF Power Amplifiers," *AEU-International Journal of Electronics and Communications* 67, no. 8 (2013): 723–728.

11. C. Li, F. You, T. Yao, et al., "Simulated Annealing Particle Swarm Optimization for High-Efficiency Power Amplifier Design," *IEEE Transactions on Microwave Theory and Techniques* 69, no. 5 (2021): 2494–2505.

12. P. Bipin and P. Rao, "Linearization of High Power Amplifier Using Modified Artificial Bee Colony and Particle Swarm Optimization Algorithm," *Procedia Technology* 25 (2016): 28–35.

13. J. A. Momoh, R. Adapa, and M. El-Hawary, "A Review of Selected Optimal Power Flow Literature to 1993. I. Nonlinear and Quadratic Programming Approaches," *IEEE Transactions on Power Systems* 14, no. 1 (1999): 96–104.

14. P. Chen, B. M. Merrick, and T. J. Brazil, "Bayesian Optimization for Broadband High-Efficiency Power Amplifier Designs," *IEEE Transactions on Microwave Theory and Techniques* 63, no. 12 (2015): 4263–4272.

15. L. Kouhalvandi, O. Ceylan, and S. Ozoguz, "Automated Deep Neural Learning-Based Optimization for High Performance High Power Amplifier Designs," *IEEE Transactions on Circuits and Systems* 67, no. 12 (2020): 4420–4433.

16. J. Kennedy and R. Eberhart, "Particle Swarm Optimization," in Proceedings of ICNN'95-International Conference on Neural Networks (IEEE, 1995), 1942–1948.

17. R. Durbin, S. R. Eddy, A. Krogh, and G. Mitchison, *Biological Sequence Analysis: Probabilistic Models of Proteins and Nucleic Acids* (Cambridge University Press, 1998).

18. M. Soruri, J. Sadri, and S. H. Zahiri, "Gene Clustering With Hidden Markov Model Optimized by PSO Algorithm," *Pattern Analysis and Applications* 21 (2018): 1121–1126.

19. M. Soruri, S. M. Razavi, M. Forouzanfar, and P. Colantonio, "Design and Fabrication of a GaN HEMT Power Amplifier Based on Hidden Markov Model for Wireless Applications," *PLoS ONE* 18, no. 5 (2023): e0285186.

20. Accessed July 10, 2024, https://www.mathworks.com/matlabcentral/fileexchange/76183-keysight-advanced-design-system-ads-to-matlab-interface.

21. Accessed July 2, 2024, https://github.com/korvin011/ADS-Matlab-Interface.

22. X. Ding, S. He, F. You, S. Xie, and Z. Hu, "2–4 GHz Wideband Power Amplifier With Ultra-Flat Gain and High PAE," *Electronics Letters* 49, no. 5 (2013): 326–327.

23. Q. H. Le, C. T. Nghe, and G. Zimmer, "High Efficiency 10 W GaN-HEMT Power Amplifier With Optimum Input Stabilization," in 2017 International Conference on Advanced Technologies for Communications (ATC) (IEEE, 2017), 27–30.

24. X. Meng, C. Yu, Y. Liu, and Y. Wu, "Design Approach for Implementation of Class-J Broadband Power Amplifiers Using Synthesized Band-Pass and Low-Pass Matching Topology," *IEEE Transactions on Microwave Theory and Techniques* 65, no. 12 (2017): 4984–4996.

25. A. S. Sayed and H. N. Ahmed, "A 10-W, High Efficiency, Broadband Harmonically Tuned GaN-HEMT Power Amplifier," in 2018 IEEE International Symposium on Circuits and Systems (ISCAS) (IEEE, 2018), 1–4.

26. N. Tuffy, A. Zhu, and T. J. Brazil, "Class-J RF Power Amplifier With Wideband Harmonic Suppression," in 2011 IEEE MTT-S International Microwave Symposium (IEEE, 2011), 1–4.

27. R. Ma, S. Goswami, K. Yamanaka, Y. Komatsuzaki, and A. Ohta, "A 40-dBm High Voltage Broadband GaN Class-J Power Amplifier for PoE Micro-Basestations," in 2013 IEEE MTT-S International Microwave Symposium Digest (MTT) (IEEE, 2013), 1–3.

28. U. Goyal, S. Tomar, M. Mishra, and S. Vinayak, "Design and Development of S Band 10 W and 20 W Power Amplifier," in 2015 IEEE Applied Electromagnetics Conference (AEMC) (IEEE, 2015), 1–2.

29. A. E. Mahdi, A. G. Sobih, and M. A. El-Kafafi, "Design and Implementation of 10 W, Highly Linear, Wideband and Efficient Power Amplifier Using Harmonic Termination," in 2016 IEEE Middle East Conference on Antennas and Propagation (MECAP) (IEEE, 2016), 1–4.